Modeling of Inner Surface Modification of a Cylindrical Tube by Plasma-Based Low-Energy Ion Implantation*

ZHENG Bocong (郑博聪), WANG Kesheng (王克胜), LEI Mingkai (雷明凯)

Surface Engineering Laboratory, School of Materials Science and Engineering,
Dalian University of Technology, Dalian 116024, China

Abstract The inner surface modification process by plasma-based low-energy ion implantation (PBLEII) with an electron cyclotron resonance (ECR) microwave plasma source located at the central axis of a cylindrical tube is modeled to optimize the low-energy ion implantation parameters for industrial applications. In this paper, a magnetized plasma diffusion fluid model has been established to describe the plasma nonuniformity caused by plasma diffusion under an axial magnetic field during the pulse-off time of low pulsed negative bias. Using this plasma density distribution as the initial condition, a sheath collisional fluid model is built up to describe the sheath evolution and ion implantation during the pulse-on time. The plasma nonuniformity at the end of the pulse-off time is more apparent along the radial direction compared with that in the axial direction due to the geometry of the linear plasma source in the center and the difference between perpendicular and parallel plasma diffusion coefficients with respect to the magnetic field. The normalized nitrogen plasma densities on the inner and outer surfaces of the tube are observed to be about 0.39 and 0.24, respectively, of which the value is 1 at the central plasma source. After a 5 μs pulse-on time, in the area less than 2 cm from the end of the tube, the nitrogen ion implantation energy decreases from 1.5 keV to 1.3 keV and the ion implantation angle increases from several degrees to more than 40°; both variations reduce the nitrogen ion implantation depth. However, the nitrogen ion implantation dose peaks of about 2×10^{10}- 7×10^{10} ions/cm^2 in this area are 2 - 4 times higher than that of 1.18×10^{10} ions/cm^2 and 1.63×10^{10} ions/cm^2 on the inner and outer surfaces of the tube. The sufficient ion implantation dose ensures an acceptable modification effect near the end of the tube under the low energy and large angle conditions for nitrogen ion implantation, because the modification effect is mainly determined by the ion implantation dose, just as the mass transfer process in PBLEII is dominated by low-energy ion implantation and thermal diffusion. Therefore, a comparatively uniform surface modification by the low-energy nitrogen ion implantation is achieved along the cylindrical tube on both the inner and outer surfaces.

Keywords: plasma-based low-energy ion implantation, inner surface modification, magnetized plasma diffusion fluid model, sheath collisional fluid model

PACS: *52.77.Dq, 52.40.Kh, 52.65.Kj*

DOI: 10.1088/1009-0630/17/4/09

(Some figures may appear in colour only in the online journal)

1 Introduction

Plasma-based ion implantation (PBII), including plasma source ion implantation (PSII) and plasma immersion ion implantation (PIII), has been demonstrated to be very effective in improving the wear and corrosion resistance for metals and alloys [1,2]. PSII was originally developed to eliminate the line-of-sight restriction of conventional ion beam implantation in 1987 [1]. Subsequently, as an alternative process to PSII, PIII which combines the features of plasma thermo-chemical diffusion treatment and ion beam implantation was reported in 1988 [2]. A high ion implantation energy from 20 keV to 100 keV in the typical range of conventional ion beam implantation is used in PBII [3,4]. At the same time, using a low ion implantation energy of about 1 keV [5,6] at elevated temperature, the technique of low-energy ion beam implantation was developed to produce similar microstructure, wear and corrosion resistance for metals and alloys, as compared with the conventional ion beam implantation.

Plasma-based low-energy ion implantation (PBLEII) combined the features of conventional PBII and low energy ion beam implantation [7,8]; lots of experimental results have shown that the PBLEII process has specific advantages over PBII and plasma thermo-chemical diffusion processing [9−12]. However, little is known about the PBLEII modification of components with a complex shape, e.g. the inner surface of a cylindrical tube, though the key technical problems such as modification

*supported by National Natural Science Foundation of China (Nos. 50725519, 51271048, 51321004)

uniformity and ion implantation depletion [13,14] could be solved in the PBLEII process using the low-energy ion implantation.

Sheridan [13] theoretically studied the inner surface modification of a cylindrical tube by PBII in 1993 and the optimization of the process was investigated by modeling the temporal sheath dynamics of the ion-matrix sheath [15−17]. In spite of successful theoretical studies of the PBII process for inner surface modification of a cylindrical tube, there is no corresponding research on the PBLEII process. In this paper, the magnetized plasma diffusion fluid model and the sheath collisional fluid model have been built to describe the nonuniform nitrogen plasma density caused by plasma diffusion during the pulse-off time and the sheath expansion and nitrogen ion implantation during the pulse-on time, respectively. Using the above models, the PBLEII process based on the design of linear electron cyclotron resonance (ECR) microwave plasma source with a magnetic field [18,19] is numerically studied.

2 PBLEII apparatus for inner surface modification of a cylindrical tube

The schematic diagram of the PBLEII apparatus for inner surface modification of a cylindrical tube is shown in Fig. 1. A linear ECR microwave plasma source and a coaxial cylindrical grounded grid electrode are arranged in a vacuum chamber, which is constructed by a metal tube component and two end flanges. The structure of the linear ECR microwave plasma source is a coaxial waveguide, which is constructed by an inner conductor of radius 0.425 cm and an outer conductor of radius 0.985 cm, and sheathed by a ceramic pipe. On the outer conductor of the coaxial waveguide, the slot antennas are slit in spirals. The position and shape of the slot antennas have been optimized to produce uniform microwave inside the tube of radius 1-10 cm and length 20-50 cm. The output power and frequency of the microwave source are 500-5000 W and 2.45 GHz, respectively. An auxiliary heating source and magnetic coils are set outside the tube: the heating source can heat the tube to 200-500 °C, and the magnetic coils are used to produce a magnetic field.

Under an external magnetic field of 0.0875 T produced by the magnetic coils, a high-density ECR microwave nitrogen plasma of about 10^{10}-10^{11} ions/cm^3 [8] can be obtained between the central plasma source and the grounded grid electrode; simultaneously the plasma diffuses through the grid to fill in the space between the inner surface of the tube and the grid and achieves a steady density distribution, which is uniform in the axial direction. When the negative voltage pulse of -0.4- -3 kV is applied onto the tube, an ion matrix sheath will be formed near its inner surface. The grounded grid electrode restricts the sheath expansion away from the central plasma source to prevent the occurrence of the hollow cathode effect. During sheath expansion, the nitrogen ions in the sheath are accelerated to implant into the surface of the tube, which is heated by the heater, to ensure the mass transfer mechanism is low-energy nitrogen ion implantation with simultaneous indiffusion, and the inner surface modification of the cylindrical tube by PBLEII is thus achieved. During the pulse-off time, the plasma around the tube tends to recover to the steady plasma density distribution. Since the low voltage bias and high electron temperature in PBLEII are beneficial to the plasma recovery, the plasma can completely recover to its steady density distribution during the pulse-off time of hundreds of μs under the typical pulse frequency of 100-1000 Hz.

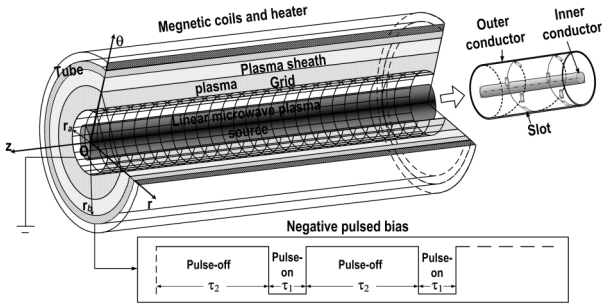

Fig.1 Schematic diagram of the plasma-based low-energy ion implantation apparatus for inner surface modification of a cylindrical tube

3 Theoretical models and calculation method

3.1 Magnetized plasma diffusion fluid model

Fig. 2 shows the schematic diagram of a cylindrical coordinate and the simulation area. Assuming that the charged coil outside the tube can generate a uniform magnetic field along the positive direction of the z axis, during the pulse-off time, the plasma produced from the central plasma source will diffuse to the tube and achieve a steady density distribution. To describe this plasma density distribution at the end of the pulse-off time, a magnetized plasma diffusion fluid model is built up based on the plasma low-pressure nonsteady diffusion fluid model [20] and by adopting a diffusion coefficient of the ion, which is verified by experiment [21]. The model details are described below.

For gas discharge plasma under working pressures ranging from low to intermediate, the effective ion velocity for ions collision with background neutrals is the ion drift velocity $|\boldsymbol{u}_\mathrm{i}|$ instead of the ion thermal velocity u_th, which means that the constant ion mobility assumption is no longer suitable. The ion mobility μ_i

depends on the ion drift velocity $|\boldsymbol{u}_\mathrm{i}|$ and can be written as [22]

$$\mu_\mathrm{i} = \frac{2q\lambda_\mathrm{i}}{\pi M\,|\mathbf{u}_\mathrm{i}|}, \tag{1}$$

where q is the ion charge, $\lambda_\mathrm{i} = 1/\ (n_\mathrm{g}\sigma_\mathrm{m})$ is the ion mean-free path, n_g is the neutral gas density, σ_m is the ion-neutral momentum transfer cross-section, and M is the mass of the ion. With a magnetic field, the ion mobility which traversed the magnetic field can be derived as [22]

$$\mu_{\perp\mathrm{i}} = \frac{\mu_\mathrm{i}}{1+(\omega_\mathrm{c}\tau_\mathrm{m})^2}, \tag{2}$$

where $\omega_\mathrm{c} = qB/M$ is the ion rotation frequency, B is the magnetic field, and $\tau_\mathrm{m} = 1/\nu_\mathrm{m}$, $\nu_\mathrm{m} = |\boldsymbol{u}_\mathrm{i}|/\lambda_\mathrm{i}$ is the ion-neutral momentum transfer frequency. For diffusion perpendicular to the magnetic field, adopting a particular diffusion coefficient $D_{\perp a} \approx \mu_{\perp\mathrm{i}}T_\mathrm{e}$, which is verified by experiment [21], the variable diffusion coefficient of the ion can be obtained as

$$D_{\perp a} \approx \mu_{\perp\mathrm{i}}T_\mathrm{e} = \frac{2qT_\mathrm{e}\lambda_\mathrm{i}}{\pi M}\frac{|\mathbf{u}_\mathrm{i}|}{|\mathbf{u}_\mathrm{i}|^2+(\omega_\mathrm{c}\lambda_\mathrm{i})^2}, \tag{3}$$

where T_e is the electron temperature. For diffusion parallel to the magnetic field, the diffusion coefficient is

$$D_a \approx \mu_\mathrm{i}T_\mathrm{e} = \frac{2qT_\mathrm{e}\lambda_\mathrm{i}}{\pi M\,|\mathbf{u}_\mathrm{i}|}. \tag{4}$$

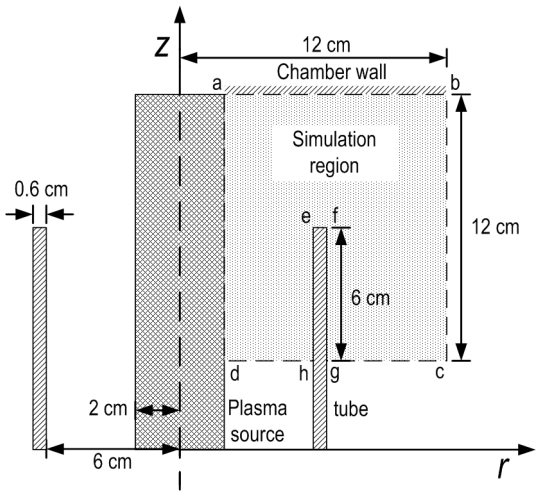

Fig.2 Schematic diagram of a cylindrical coordinate and the simulation area

Substituting the ion flux $\Gamma = -\boldsymbol{D}\nabla n_\mathrm{i}$ into the equation of ion continuity yields

$$\frac{\partial n_\mathrm{i}}{\partial t} + \nabla\cdot(\Gamma) = 0. \tag{5}$$

Then Eq. (5) becomes

$$\frac{\partial n_\mathrm{i}}{\partial t} - \nabla\cdot(\mathbf{D}\nabla n_\mathrm{i}) = 0. \tag{6}$$

where n_i is the ion density, and $\boldsymbol{D}$ is the diffusion coefficient composed of $D_{\perp a}$ and D_a. Together with the ion motion equation

$$\frac{\partial \mathbf{u}_\mathrm{i}}{\partial t} = -\mathbf{u}_\mathrm{i}\cdot\nabla\mathbf{u}_\mathrm{i} + \frac{q}{M}(E+\mathbf{u}_\mathrm{i}\times\mathbf{B}) - \frac{qT_\mathrm{i}}{M}\frac{\nabla n_\mathrm{i}}{n_\mathrm{i}} - \frac{\mathbf{F}_\mathrm{c}}{M}, \tag{7}$$

where t is time, T_i is the ion temperature, the electric field $\boldsymbol{E}$ obtained from Boltzmann's distribution of electrons is

$$\mathrm{E} = -T_\mathrm{e}\frac{\nabla n_\mathrm{i}}{n_\mathrm{i}}, \tag{8}$$

and the collisional drag force $\mathbf{F}_\mathrm{c}$ is [23]

$$\mathbf{F}_\mathrm{c} = \frac{\pi}{2}M\nu_\mathrm{m}\mathbf{u}_\mathrm{i}. \tag{9}$$

Substituting Eqs. (8) and (9) into the ion motion Eq. (7), then

$$\frac{\partial \mathbf{u}_\mathrm{i}}{\partial t} = -\mathbf{u}_\mathrm{i}\cdot\nabla\mathbf{u}_\mathrm{i} - \frac{q\,(T_\mathrm{e}+T_\mathrm{i})}{M}\frac{\nabla n_\mathrm{i}}{n_\mathrm{i}} + \frac{q}{M}\mathbf{u}_\mathrm{i}\times\mathbf{B} - \frac{\pi}{2}\nu_\mathrm{m}\mathbf{u}_\mathrm{i}. \tag{10}$$

The magnetized plasma diffusion fluid model, which is composed of Eqs. (6) and (10), can be used to describe the diffusion behavior of magnetized plasma. The diffusion coefficient perpendicular to the magnetic field is in good agreement with measured values for a range of magnetic fields and gas pressures [21]; without the magnetic field, the model degrades to the plasma low-pressure nonsteady diffusion fluid model [20], which has been verified to be accurate when compared with the particle-in-cell method [24]. Therefore, the magnetized plasma diffusion fluid model is acceptable to describe the magnetized plasma diffusion behavior. The mathematical description of the model in two dimensional cylindrical coordinates can be represented as

$$\begin{aligned}
\frac{\partial n_\mathrm{i}}{\partial t} &= \frac{2qT_\mathrm{e}\lambda_\mathrm{i}}{\pi M}\frac{1}{r}\frac{\partial}{\partial r}\left(\frac{r}{|\mathbf{u}_\mathrm{i}|}\frac{\partial n_\mathrm{i}}{\partial r}\right) \\
&\quad + \frac{2qT_\mathrm{e}\lambda_\mathrm{i}}{\pi M}\frac{\partial}{\partial z}\left(\frac{|\mathbf{u}_\mathrm{i}|}{|\mathbf{u}_\mathrm{i}|^2+(\omega_c\lambda_\mathrm{i})^2}\frac{\partial n_\mathrm{i}}{\partial z}\right); \\
\frac{\partial u_r}{\partial t} &= -u_r\frac{\partial u_r}{\partial r} - u_z\frac{\partial u_r}{\partial z} + \frac{u_\vartheta^2}{r} \\
&\quad - \frac{q\,(T_\mathrm{e}+T_\mathrm{i})}{Mn_\mathrm{i}}\frac{\partial n_\mathrm{i}}{\partial r} + \frac{q}{M}u_\vartheta B - \frac{\pi}{2}\frac{1}{\lambda_\mathrm{i}}|\mathbf{u}_\mathrm{i}|\,u_r; \\
\frac{\partial u_\vartheta}{\partial t} &= -u_r\frac{\partial u_\vartheta}{\partial r} - u_z\frac{\partial u_\vartheta}{\partial z} - \frac{u_\vartheta u_r}{r} - \frac{q}{M}u_r B - \frac{\pi}{2}\frac{1}{\lambda_\mathrm{i}}|\mathbf{u}_\mathrm{i}|\,u_\vartheta; \\
\frac{\partial u_z}{\partial t} &= -u_r\frac{\partial u_z}{\partial r} - u_z\frac{\partial u_z}{\partial z} - \frac{q\,(T_\mathrm{e}+T_\mathrm{i})}{Mn_\mathrm{i}}\frac{\partial n_\mathrm{i}}{\partial z} - \frac{\pi}{2}\frac{1}{\lambda_\mathrm{i}}|\mathbf{u}_\mathrm{i}|\,u_z,
\end{aligned} \tag{11}$$

where $|\boldsymbol{u}_\mathrm{i}| = (u_r^2+u_\vartheta^2+u_z^2)^{1/2}$, and u_r, u_ϑ, u_z are the components of $\boldsymbol{u}_\mathrm{i}$ in the radial, tangential and axial directions, respectively.

3.2 Sheath collisional fluid model

During the pulse-on time, a relatively high pulsed bias is applied onto the tube; the equations described the temporal behavior of ions in the sheath, which are ion continuity, ion motion, Poisson's equation and Boltzmann's relationship of electrons, as follows

$$\begin{aligned}
&\frac{\partial n_{\mathrm{i}}}{\partial t}+\nabla\cdot\left(n_{\mathrm{i}}\cdot\mathbf{u}_{\mathrm{i}}\right)=0;\\
&\frac{\partial\mathbf{u}_{\mathrm{i}}}{\partial t}+\left(\mathbf{u}_{\mathrm{i}}\cdot\nabla\right)\mathbf{u}_{\mathrm{i}}=\frac{q}{M}\left(-\nabla\varphi+\mathbf{u}_{\mathrm{i}}\times B\right)-\frac{\mathbf{F}_{\mathrm{c}}}{M};\\
&\nabla^2\varphi=-\frac{q}{\varepsilon_0}\left(n_{\mathrm{i}}-n_{\mathrm{e}}\right);\\
&n_{\mathrm{e}}=n_0\exp\left(\varphi/T_{\mathrm{e}}\right).
\end{aligned}\tag{12}$$

In the above equations, φ is the electric potential, n_0 is the plasma source density, and ε_0 is the permittivity of free space. The mathematical description in two dimensional cylindrical coordinates can be represented as

$$\begin{aligned}
&\frac{\partial n_{\mathrm{i}}}{\partial t}+\frac{1}{r}\frac{\partial}{\partial r}\left(rn_{\mathrm{i}}u_r\right)+\frac{\partial}{\partial z}\left(n_{\mathrm{i}}u_z\right)=0;\\
&\frac{\partial u_r}{\partial t}+u_r\frac{\partial u_r}{\partial r}+u_z\frac{\partial u_r}{\partial z}=\frac{u_\vartheta^2}{r}+\frac{q}{M}\left(-\frac{\partial\varphi}{\partial r}+u_\vartheta B\right)\\
&\qquad\qquad-\frac{\pi}{2}\frac{1}{\lambda_{\mathrm{i}}}\left|\mathbf{u}_{\mathrm{i}}\right|u_r;\\
&\frac{\partial u_\vartheta}{\partial t}+u_r\frac{\partial u_\vartheta}{\partial r}+u_z\frac{\partial u_\vartheta}{\partial z}=-\frac{u_\vartheta u_r}{r}-\frac{q}{M}u_rB-\frac{\pi}{2}\frac{1}{\lambda_{\mathrm{i}}}\left|\mathbf{u}_{\mathrm{i}}\right|u_\vartheta;\\
&\frac{\partial u_z}{\partial t}+u_r\frac{\partial u_z}{\partial r}+u_z\frac{\partial u_z}{\partial z}=-\frac{q}{M}\frac{\partial\varphi}{\partial z}-\frac{\pi}{2}\frac{1}{\lambda_{\mathrm{i}}}\left|\mathbf{u}_{\mathrm{i}}\right|u_z;\\
&\frac{1}{r}\frac{\partial}{\partial r}\left(r\frac{\partial\varphi}{\partial r}\right)+\frac{\partial^2\varphi}{\partial z^2}=-\frac{q}{\varepsilon_0}\left(n_{\mathrm{i}}-n_0\exp\left(\frac{\varphi}{T_{\mathrm{e}}}\right)\right).
\end{aligned}\tag{13}$$

3.3 Calculation method and boundary conditions

The simulation area is shadowed in Fig. 2. The axis of the cylindrical coordinate coincides with the central axis of the tube, 6.0 cm inside the tube and 6.0 cm outside the tube, the inner radius of the tube r_b is 6.0 cm and the tube wall thickness is 0.6 cm. The top boundary ab is the chamber wall, the bottom cd is the symmetric boundary, the left side ad is the central plasma source boundary and the right side bc is the free boundary. The models are numerically solved by the finite difference method under a 0.0875 T magnetic field. In the simulation, the typical PBLEII parameters are adopted as [8]: grid radius r_a= 2 cm, central microwave plasma source density $n_0 = 1.0 \times 10^{10}$ ions/cm^3, electron temperature $T_{\mathrm{e}} = 8$ eV, and negative pulsed voltage $\varphi_{\mathrm{p}} = -2$ kV. The pulse-on time τ_1 is set as 5 μs during the calculation, the pulse-off time τ_2 is sufficiently long for the plasma to recover to its steady state under the typical pulse frequency of 100-1000 Hz in PBLEII so that the specific value of τ_2 is unimportant. The processing pressure of pure nitrogen P is 5×10^{-2} Pa, the positive ion in the plasma is nitrogen molecular ion N_2^+, and the treated tube is steel.

The momentum transfer cross-section σ_{m} between N_2^+ and the neutral nitrogen molecule is fitted by experimental data [25] as

$$\begin{cases}
\sigma_{\mathrm{m}}=\left(56.46+\frac{38.34}{\sqrt{\varepsilon}}\right)\times10^{-20}\ \mathrm{m}^2 & \varepsilon\geq10^{-4}\ \mathrm{eV}\\
\sigma_{\mathrm{m}}=3.89\times10^{-17}\ \mathrm{m}^2 & \varepsilon<10^{-4}\ \mathrm{eV}
\end{cases},\tag{14}$$

where ε is the energy of N_2^+ in eV.

For the magnetized plasma diffusion fluid model, assuming that a plasma density of n_0 can be provided by the central plasma source continuously, the boundary condition on the radius of the central plasma source is

$$n_{\mathrm{i}}|_{r=r_a}=n_0.\tag{15}$$

Before the bias is applied, there will be a floating sheath formed on the tube surface as well as on the chamber wall. The electric force dominates the magnetic Lorentz force as one approaching the plasma boundary [26], therefore, the ion flux near the inner surface can be written as $\Gamma=-D_a\nabla n_{\mathrm{i}}$, where $D_a \approx \mu_{\mathrm{i}}T_{\mathrm{e}}$ is the plasma's ambipolar diffusion coefficient in the absence of a magnetic field. Ignoring the floating sheath thickness, the ion velocity at the tube and the chamber wall is the Bohm velocity

$$u_{\mathrm{B}}=-D_a\left.\frac{\nabla n_{\mathrm{i}}}{n_{\mathrm{i}}}\right|_{\mathrm{ab,he,ef,fg}},\tag{16}$$

then the boundary condition on the tube surface and the chamber wall can be derived from Eq. (16) as

$$\nabla n_{\mathrm{i}}|_{\mathrm{ab,he,ef,fg}}=-\frac{\pi}{2}\frac{n_{\mathrm{i}}}{\lambda_{\mathrm{i}}}.\tag{17}$$

The symmetric boundary condition on the bottom boundary cd is $\partial n_{\mathrm{i}}/\partial z = 0$, and the free boundary condition on the right boundary bc is $\partial^2 n_{\mathrm{i}}/\partial r^2 = 0$. During the calculation, the space step and time step are taken as 0.1 cm and 0.4 ns, respectively, and the diffusion process is assumed to achieve the steady state when the change of the normalized ion density in the simulation area in 1 μs is less than 10^{-4}.

For the sheath collisional fluid model, the initial plasma density is obtained from the magnetized plasma diffusion fluid model, and the initial electric potential in the simulation area is $\varphi = 0$. The boundary conditions are $\varphi=\varphi_{\mathrm{p}}$ on the tube, $\varphi = 0$ on the chamber wall and central source, and $\nabla\varphi$=0 on the boundary of bc and cd. During the calculation, the sheath boundary is set at the location where $\varphi/\varphi_{\mathrm{p}} = 10^{-2}$, the space step and time step are taken as 0.1 cm and 4 ns, respectively.

4 Results and discussion

4.1 Evolution of plasma density and sheath

Fig. 3 demonstrates the normalized nitrogen plasma density distribution at the end of the pulse-off time in the simulation area calculated by the magnetized plasma diffusion fluid model. It can be seen that the plasma density is not uniform and decreases significantly far away from the central plasma source along the radial direction, since the plasma diffusion is reduced as it traverses the magnetic field. However, the plasma diffusion parallel to the magnetic field is not reduced; the density distribution along the axial direction is comparatively uniform even in the area outside the tube where the radial diffusion is hindered by the tube wall. The normalized nitrogen plasma densities on the inner and outer surface of the tube are observed to be about 0.39 and 0.24, respectively, while the normalized density is 1 at the central plasma source ad.

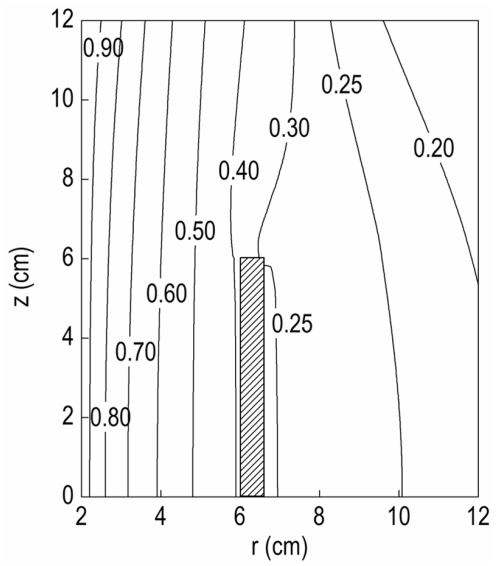

Fig.3 The normalized nitrogen plasma density distribution in the simulation area at the end of the pulse-off time

Using the above result as the initial plasma density distribution, the sheath expansion during the pulse-on time is investigated by the sheath collisional fluid model. Fig. 4 shows the sheath evolution during a 5 μs pulse-on time in the simulation area. Under the uniform plasma density distribution, the sheath expansion on the inner surface of the tube should be faster than that on the outer surface, since the ions entering into the sheath decrease on the inner side and increase on the outer side of the tube as the sheath expands [27]. However, due to the plasma nonuniformity caused by diffusion, the plasma density is higher on the inner surface of the tube, and the sheath thickness is slightly thinner compared with that on the outer surface. The sheath expands slower at the end of the tube, since there are more ions entering into the sheath.

Fig. 5 shows the corresponding normalized nitrogen ion density distribution at different pulse-on times. Compared with the initial plasma density distribution, it can be seen that the ion densities remain unchanged outside the sheath, and decrease significantly in the sheath region around the tube wall due to the acceleration induced by the sheath's electric field. The ion density in front of the inner and outer surfaces of the tube is uniform, however, a local maximum of ion density appears at the end of the tube due to the ion focusing. The influence of this phenomenon on the ion implantation process will be described in the following sections.

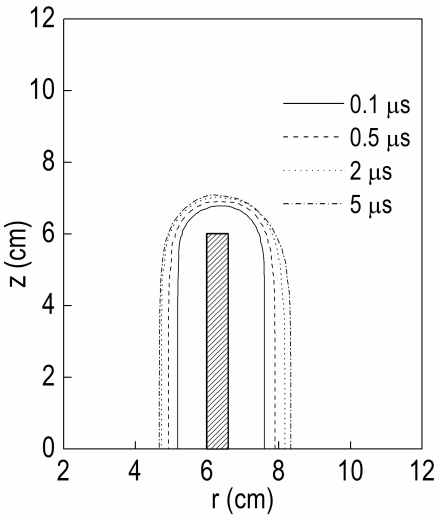

Fig.4 Sheath evolution during a 5 μs pulse-on time in the simulation area

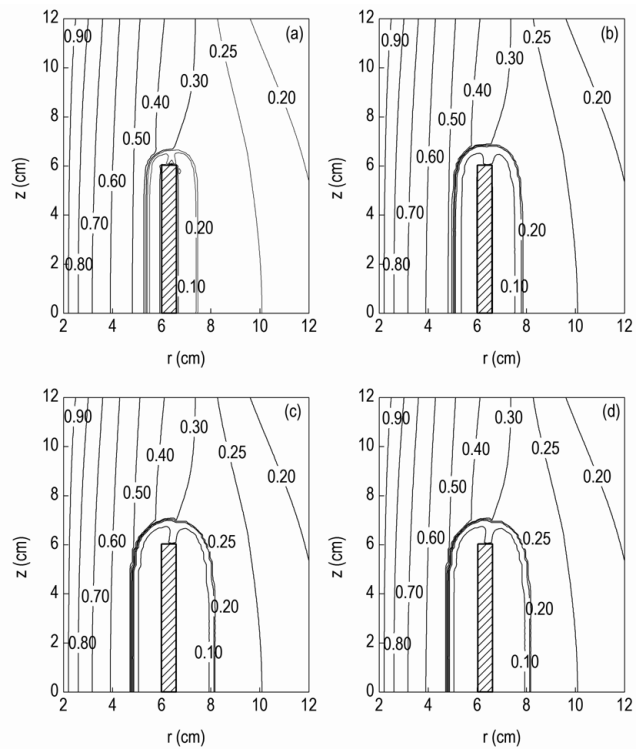

Fig.5 Normalized nitrogen ion density distribution in the simulation area at the pulse-on times of (a) 0.1 μs, (b) 0.5 μs, (c) 2 μs, and (d) 5 μs

4.2 Ion implantation energy and angle

Fig. 6 shows the nitrogen ion implantation energy distribution along the tube surface at different pulse-on times. The horizontal position is from the point h in Fig. 2, along the inner surface he, through the tube end ef, to the outer surface fg. It can be seen that the implantation energy increases rapidly during the initial pulse-on time, from about 0.8 keV at 0.1 μs up to 1.4 keV at 0.5 μs, then it increases gradually and stabilizes at around 1.5 keV after 2 μs. The spatial distribution of energy is uniform on the inner and outer surfaces, and the energy decreases toward the end of the tube from 1.5 keV to 1.3 keV. The energy decrease should be due to the sheath deformation at the end of the tube, resulting in a longer ion transport distance through the sheath, and the ions experience more collision with neutral gas and the energy is thus reduced. The low ion implantation energy near the end of the tube results in a relatively thin implantation depth, therefore, the implantation depth near the end of the tube would be less than that on the middle part of the tube from the viewpoint of ion implantation energy.

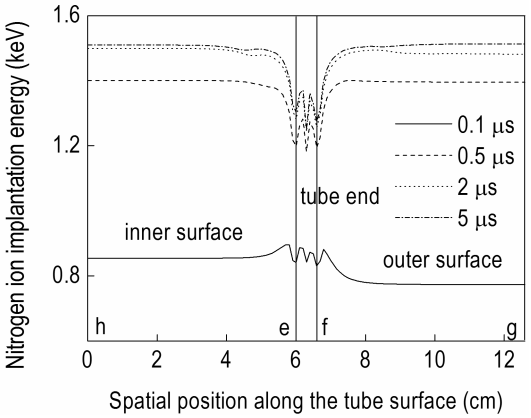

Fig.6 The nitrogen ion implantation energy distribution along the tube surface at different pulse-on times

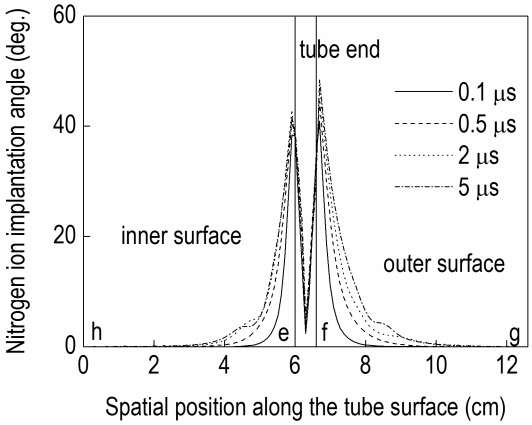

Fig.7 The nitrogen ion implantation angle distribution along the tube surface at different pulse-on times

Fig. 7 shows the nitrogen ion implantation angle distribution along the tube surface at different pulse-on times. The ion implantation angle is defined as the incline angle between the direction of ion implantation velocity and the normal direction of the tube surface, namely the degree is zero when the ion implants in the normal direction. The mathematical description of the implantation angle is

$$\eta = \arctan\left(\frac{\sqrt{u_z^2 + u_\vartheta^2}}{u_r}\right). \tag{18}$$

The implantation angle near the end of the tube has two maximal peaks, which are more than 40°, and decreases rapidly to several degrees far away from the end. The large ion implantation angle near the end of the tube may result in a relatively strong sputtering, which is not beneficial to the ion implantation. Therefore, the modification effect near the end of the tube would not be as good as that on the middle part of the tube from the viewpoint of the ion implantation angle as well.

4.3 Ion implantation flux and dose

Fig. 8 shows the nitrogen ion implantation flux distribution along the tube surface at different pulse-on times. The ion implantation flux on the tube surface is defined as

$$\Gamma = n_\mathrm{i}\,|\mathbf{u}_\mathrm{i}|\cos\eta. \tag{19}$$

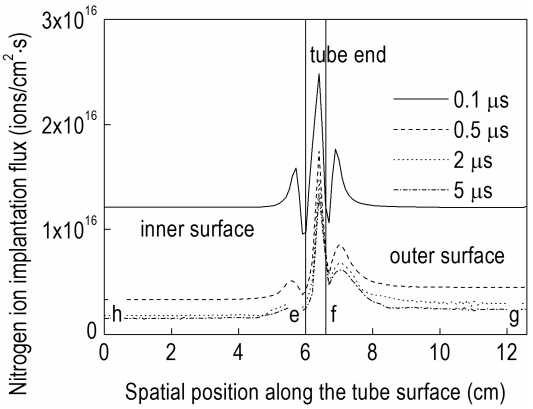

Fig.8 The nitrogen ion implantation flux distribution along the tube surface at different pulse-on times

During the pulse-on time, the ion implantation flux increases at first then decreases, and tends to a steady state. The flux is uniform along the inner and outer surface of the tube, and three flux peaks appeared near the end of the tube due to the ion focusing caused by sheath deformation. This is similar to the process of inner surface modification of a tube by conventional PBII [27]. Under uniform plasma density, the ion flux on the outer surface of the tube should be much higher than that on the inner surface, since the ions tend to be dispersed on the inner surface and concentrated on the outer surface. However, the plasma is nonuniform around the tube wall, and there is no significant difference of ion implantation flux between the inner and outer surfaces of the tube. Fig. 9 shows the nitrogen ion implantation dose distribution along the tube surface at different pulse-on times. Here, assuming that all

the ions impacting on the inner surface can implant into the surface during the pulse-on time, the ion implantation dose D can be obtained from the time integration of the ion implantation flux

$$D = \int_0^t \Gamma \cdot \mathrm{d}t \tag{20}$$

From Fig. 9, it can be seen that the dose distribution along the tube surface is similar to the flux distribution. The ion implantation dose during a 5 μs pulse are obtained as about 1.18×10^{10} ions/cm^2 and 1.63×10^{10} ions/cm^2 on the inner and outer surfaces of the tube, and three dose peaks of about 2×10^{10}-7×10^{10} ions/cm^2 appeared near the end of the tube. Compared with a conventional PBII process, the central plasma source can provide plasma continuously and the ion implantation depletion on the inner surface of the tube can be avoided in the PBLEII process.

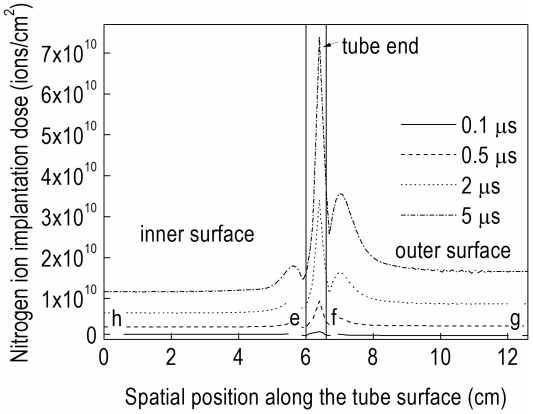

Fig.9 The nitrogen ion implantation dose distribution along the tube surface at different pulse-on times

The above results demonstrate that in the area less than 2 cm from the end of the tube, the nitrogen ion implantation energy decreases from 1.5 keV to 1.3 keV and the ion implantation angle increases from several degrees to more than 40°, both variations reduce the nitrogen ion implantation depth. However, in this area, the implantation dose peaks of about 2×10^{10} - 7×10^{10} ions/cm^2 during a 5 μs pulse are 2 - 4 times higher than the implantation dose of 1.18×10^{10} ions/cm^2 and 1.63×10^{10} ions/cm^2 on the inner and outer surfaces of the tube. Different from the conventional PBII process, the sufficient ion implantation dose ensures an acceptable modification effect near the end of the tube under the low energy and large angle conditions for nitrogen ion implantation, because the modification effect is mainly determined by the ion implantation dose as the mass transfer process in PBLEII is dominated by low-energy ion implantation and thermal diffusion. Therefore, a comparatively uniform surface modification by the low-energy nitrogen ion implantation is achieved along the cylindrical tube on both the inner and the outer surfaces. Compared with other inner surface modification processes, e.g., grid enhanced plasma source ion implantation (GEPSII) [17], the requirement of power supply is weakened since the mass transfer mechanism in the PBLEII technique is low-energy ion implantation and simultaneous indiffusion, and thus the low pulsed bias can be applied onto the target instead of high pulsed bias, and power waste and x-ray radiation due to the strong secondary electron emission caused by the high pulsed bias can be avoided. Therefore, PBLEII is a low-cost, environmentally friendly surface processing technique, which has broad industrial application prospects in the science branch of surface engineering.

5 Conclusions

a. In order to optimize the low-energy ion implantation parameters for industrial applications, the magnetized plasma diffusion fluid model and sheath collisional fluid model are successfully used to study the inner surface modification process by plasma-based low-energy ion implantation (PBLEII) with an electron cyclotron resonance (ECR) microwave plasma source located at the central axis of a cylindrical tube.

b. At the end of the pulse-off time, the plasma density around the tube is nonuniform caused by the plasma diffusion. Moreover, the nonuniformity is more apparent along the radial direction compared with that along the axial direction due to the geometry of the linear plasma source in the center and the difference between perpendicular and parallel plasma diffusion coefficients with respect to the magnetic field line. The normalized nitrogen plasma densities on the inner and outer surfaces of the tube are observed to be about 0.39 and 0.24, respectively, while the normalized density is 1 at the central plasma source.

c. After a 5 μs pulse-on time, in the area less than 2 cm from the end of the tube, the nitrogen ion implantation energy decreases from 1.5 keV to 1.3 keV, the ion implantation angle increases from several degrees to more than 40°, and the implantation dose peaks in this area are 2 - 4 times higher than those on other places. The sufficient ion implantation dose ensures an acceptable modification effect near the end of the tube under the low energy and large angle conditions for nitrogen ion implantation, because the modification effect is mainly determined by the ion implantation dose, as the mass transfer process in PBLEII is dominated by low-energy ion implantation and thermal diffusion. Therefore, a comparatively uniform surface modification by the low-energy nitrogen ion implantation is achieved along the cylindrical tube on both the inner and the outer surfaces.

References

1 Conrad J R. 1987, J. Appl. Phys., 62: 777
2 Tendys J, Donnelly I J, Kenny M J, et al. 1988, Appl. Phys. Lett., 53: 2143
3 Leutenecker R, Wagner G, Louis T, et al. 1989, Mater. Sci. Eng. A, 115: 229

4 Williamson D L, Wang L, Wei R, et al. 1990, Mater. Lett., 9: 302
5 Byeli A V, Shikh S K, Khatko V V. 1992, Wear, 159: 185
6 Williamson D L, Ozturk O, Wei R, et al. 1994, Surf. Coat. Technol., 65: 15
7 Lei M K, Zhang Z L. 1995, J. Vac. Sci. Technol. A, 13: 2986
8 Lei M K, Zhang Z L, Ma T C. 2000, Surf. Coat. Technol., 131: 317
9 Barradas N P, Maas A J H, Mändl S, et al. 1997, Surf. Coat. Technol., 93: 238
10 Mukherjee S, Chakraborty J, Gupta S, et al. 2002, Surf. Coat. Technol., 156: 103
11 Sarapirom S, Sangwijit K, Anuntalabhochai S, et al. 2002, Surf. Coat. Technol., 156: 103
12 Rao K R M, Mukherjee S, Raole P M, et al. 2005, Surf. Coat. Technol., 200: 2049
13 Sheridan T E. 1993, J. Appl. Phys., 74: 4903
14 Sun M, Yang S Z, Li B. 1996, J. Vac. Sci. Technol. A, 14: 367
15 Wang J L, Zhang G L, Fan S H, et al. 2003, J. Phys. D, 36: 1192
16 Zeng X C, Kwok T K, Liu A G, et al. 1998, J. Appl. Phys., 83: 44
17 Li Y, Zheng B C, Lei M K. 2012, Vacuum, 86: 1278
18 Glukhoy Y, Rahman M, Popov G, et al. 2005, Surf. Coat. Technol., 196: 172
19 Lei M K, Ou Y X, Wu Z L, et al, China Patent, CN 101713065A
20 Li Y, Zheng B C, Lei M K. 2013, IEEE. Trans. Plasma Sci., 41: 43
21 Vidal F, Johnston T W, Margot J, et al. 1999, IEEE. Trans. Plasma Sci., 27: 727
22 Lieberman M A, Lichtenberg A J. 2005, Principles of plasma discharges and materials processing (Second Edition). John Wiley & Sons Inc, New Jersey
23 Sheridan T E, Goeckner M J. 1995, J. Appl. Phys., 77: 4967
24 Wood B P. 1993, J. Appl. Phys., 73: 4770
25 Phelps A V. 1991, J. Phys. Chem. Ref. Data, 20: 557
26 Allen J E. 2007, Phys. Plasmas, 14: 024701
27 Liu C S, Wang D Z. 2003, Acta Phys. Sin.-Ch. Ed., 52: 109 (in Chinese)

(Manuscript received 9 June 2014)
(Manuscript accepted 21 August 2014)
E-mail address of corresponding author
LEI Mingkai: surfeng@dlut.edu.cn